The Effects of Spinning Conditions on Asymmetric 6FDA/6FDAM Polyimide Hollow Fibers for Air Separation

TAI-SHUNG CHUNG,[1,2] E. RONALD KAFCHINSKI[3]

[1] Department of Chemical Engineering, [2] Institute of Materials Research and Engineering, National University of Singapore, Republic of Singapore 0511

[3] Hoechst Celanese Research Division, 86 Morris Avenue, Summit, New Jersey 07961

Received 7 May 1996; accepted 29 October 1996

ABSTRACT: We have found that the chemistries of inner and external coagulants, gelation bath temperature, and air gap distance have profound effects on 6FDA-polyimde hollow-fiber morphology and performance. This 6FDA-polyimide is made of 50 mol % 2,2′-bis(3,4′-dicarboxyphenyl) hexafluoro propane dianhydride (6FDA) and 50 mol % 2,2′-bis(3-aminophenyl) hexafluoro propane (4,4′ 6F-diamine) (6FDAM). An increase in air gap distance tends to induce three-dimensional open-cell pore formation. Raising bath temperature has a similar effect. Multilayer finger-void structure can be completely eliminated if one properly chooses a bore-fluid flow rate and a gelation bath temperature. Experimental data demonstrate that the location of the dense layer can be shifted from the inner skin to the outer skin based on the chemistry (solubility parameter) of coagulants. The location of finger voids is also dependent on the chemistry of coagulants, and the dense layer location may shift from the inner surface to the external surface or appear in both surfaces dependent on the differences in solubility and coagulation rate. A defect-free 6FDA/6FDAM polyimide fiber with a selectivity of 4.73 and a permeance of 38.1 GPU is produced. © 1997 John Wiley & Sons, Inc. J Appl Polym Sci **65:** 1555–1569, 1997

Key words: 6FDA polyimide membranes; hollow-fiber membrane; phase-inversion process; air separation

INTRODUCTION

The development of asymmetric membranes for air/gas separation has received significant attention from both academia and industry. This is due to the fact that air/gas separation membranes have tremendous business potential. Significant advancement has been made in both membrane materials and fabrication technology during the last 15 years. Materials with better separation characteristics, i.e., permeability and selectivity, such as 6FDA-polyimides and tetrabromobisphenol A polycarbonates, have been discovered.[1–6] Some of them have selectivities greater than 7.5 for O_2/N_2 with permeabilities of O_2 over one barrer at room temperature. Various membrane fabrication techniques have been invented. Researchers at Permea (now belongs to Air Products) led the breakthroughs and developed the second-generation polysulfone hollow fibers using Lewis acid : base complex solvent technology.[7,8] This technology has been examined, evaluated, and expanded by Chung and his coworkers[9] at Hoechst Celanese (HC). They found that the boundary value set by Permea for the Hildebrand parameter was not appropriate. Researchers at HC also simplified the overall spinning process by spinning fibers directly from *in situ* polymeriza-

Correspondence to: T-S Chung.

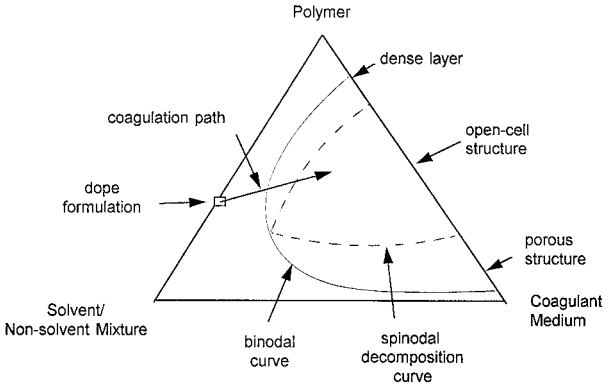

Figure 1 A typical phase diagram for a ternary system and the coagulation path during the precipitation of a hollow fiber at a constant temperature.[9,14–18]

tion (imidization) dopes and completely eliminating the time and complexity for dope preparation. They demonstrated that, for the first time, a defect-free 6FDA-polyimide hollow fiber could be produced from modified Lewis acid : base complex dopes.[10] A research group at the University of Texas (UT) developed extrathin defect-free asymmetric flat membranes using special solvent/nonsolvent systems and forced convective evaporation technology.[11] Both HC and UT technologies do not require an additional silicone coating to seal fiber defects. Silicone curing is a secondary operation that adds cost, time, and complexity to the membrane fabrication process.

In fact, the fundamentals of asymmetric membrane technology for air/gas separation membranes are extensions of the Loeb-Sourirajan technique[12] developed for reverse osmosis (RO) applications about 30 years ago. However, the selective layer in air/gas separation membranes has to have a much higher degree of perfection than that in RO membranes. The pore size required for air separation membranes is usually about 1–5 Å, which is significantly smaller than that for RO membranes (3–15 Å). RO membranes are generally considered defective for air separation because their pore sizes are too big to distinguish between O_2 and N_2 molecules and they do not show useful (or any) selectivity for air separation.[13]

LITERATURE REVIEW

The fabrication of an air-separation hollow-fiber membrane with a desirable pore-size distribution and performance is not a trivial process. There are many factors controlling fiber morphology during the phase inversion. The formation of asymmetric membranes has been studied and reviewed by many authors.[13–21] However, most attention has been given to either RO, ultrafiltration (UF), and microfiltration (MF) membranes or asymmetric flat air-separation membranes. Because the separation mechanisms of RO, UF, MF, and air-separation membranes are different and they have quite different pore sizes (various from 1–5 Å to 1 μm), the knowledge developed for RO, UF, and MF membranes is relatively limited when applied it to develop high-performance air-separation membranes. Nevertheless, it provides us with useful experience and scientific principles to qualitatively understand the phase-inversion process during the formation of air-separation membranes.

Flat air-separation membranes are usually prepared by casting a polymeric solution on a substrate and convective dried for a short period of time before immersing in a nonsolvent coagulation bath. Many research groups have analyzed this technology in depth.[17,20,21] However, the mechanism for asymmetric hollow-fiber formation is much more complicated than those for asymmetric flat membranes. For example, it is a known fact that it is very difficult to simulate the hollow-fiber spinning process by adopting the process conditions developed for asymmetric flat membranes. The controlling factors for hollow-fiber morphology are different from those for flat membranes. There are two coagulations taking place in hollow-fiber spinning (internal and external surfaces), while there is only one major coagulation surface for an asymmetric flat sheet membrane. If liquids are used as bore fluids, the internal coagulation process for a hollow fiber starts immediately after extrusion from a spinneret and then the fiber goes through the external coagulation, while there is usually a waiting period for an asymmetric flat membrane before immersing it into a coagulant. Depending on the membrane wall thickness and solvent exchange rate, the formations of inner and outer skins of a hollow fiber are more interrelated than those of a flat membrane. In addition, the spinning dopes suitable

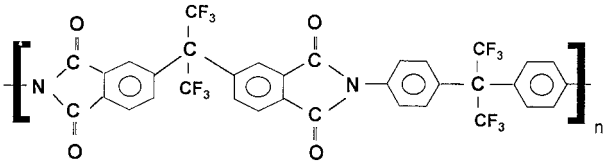

Figure 2 Chemical structure of the 6FDA/6FDAM polyimide.

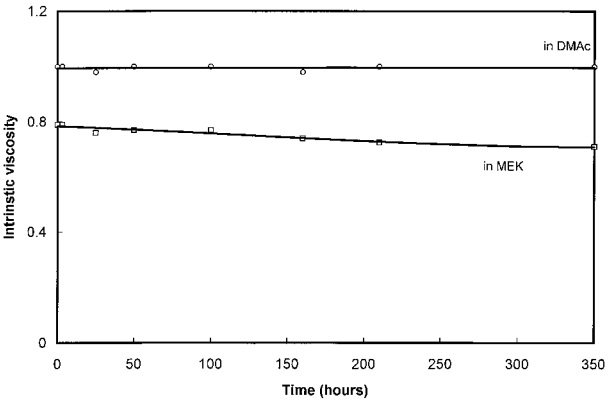

Figure 3 Dope stability (intrinsic viscosity) as a function of solvents and time (○: DMAc, □: MEK).

for hollow-fiber fabrication generally have much greater viscosity and elasticity than those for flat membranes. This high viscosity retards solvent exchange rates and introduces complexity during the precipitation. Because hollow-fiber formation is usually done nonisothermally under tension, the Gibbs free energies for the states of spinning solutions (for hollow fibers) and casting solutions (for flat membranes) are different.[22] Chung suggested that the Gibbs free energy of a polymeric solution in an isothermal hollow-fiber spinning under tension may have two more terms than that in a casting process: one is a work, done by the external stresses to the as-spun nascent fiber, and the other is an extra entropy change,

$$\frac{\Delta S^{\text{extra}}}{RT}$$

induced by these stresses.[22] For air-separation hollow-fiber membranes, Kesting and his coworkers reported that coagulation rates and solvent exchange mechanisms were strongly dependent on their respective molecular sizes and solubility differences.[7,23] The bigger the molecular size is, the slower the exchange process will be. An increase in the solubility difference between dope solvents and coagulants results in an increase in coagulation rate. Therefore, the most important step to yield a good fiber is to select appropriate solvents and nonsolvents (coagulants) for the spinning dope. In addition to the solvent selection, Chung et al. analyzed previous work on dope formulations for air-separation membranes and concluded that the keys to prepare high-performance air-separation membranes were to prepare dopes having a decomposition curve very close to the axis of polymer–solvent/nonsolvent mixture (Fig. 1) and to eliminate the inner dense layer using a low coagulation-power bore-fluid.[9] If the phase separation curve is moved very close to the left axis, the as-spun fiber can be coagulated in the early stage of precipitation as quickly as possible at controlled environments. In fact, this idea has been often practiced in both academia and industry for the development of gas-separation membranes.[6,10,24,25] Viscosity also plays an important role on fiber performance. Experimental data implied that spinning dopes with a viscosity in the region of chain entanglement seemed to be essential to yield hollow fibers with minimum defects.[9]

Although various hollow-fiber membranes for air separation have been developed, most publications have emphasized on the product development, and very rarely has attention been given to systematically study the relationship among fiber morphology, performance, and process conditions. Pesek and Koros may be the pioneers in this area[26,27]; however, their experimental design focused on the effect of spinning conditions on fiber separation performance. In this article, we would like to explore this relationship and emphasize our research on the effect of spinning conditions on asymmetric hollow-fiber morphology. A 6FDA-polyimide material is used in this study.

EXPERIMENTAL APPROACHES

Materials

The 6FDA/6FDAM polyimide polymer used had an intrinsic viscosity (IV) of 1.0 in 0.5 wt % DMAc (*N,N*-dimethylacetamide). This polyimide was synthesized by Mr. R. H. Vora in Hoechst Celanese. Figure 2 illustrates the chemical structure of this hexafluoro–isopropylidene group-con-

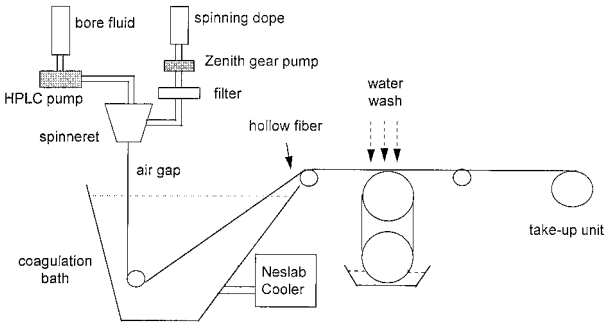

Figure 4 Schematic diagram of a hollow-fiber spinning line.

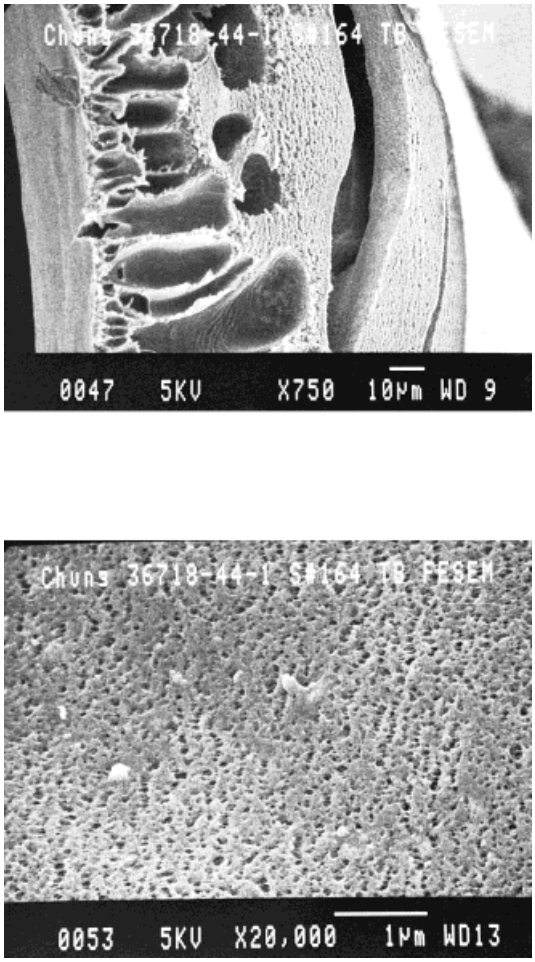

Figure 5 SEM pictures of the cross-section and external surface of fibers precipitated in 3–4°C (internal coagulant = 80/20 acetone/water, external coagulant = 20/80 DMAc/MeOH, 2.54 cm air-gap). Magnification: ×750 (top) and ×20,000 (bottom).

taining polyimide. It was synthesized using solution poly-condensation reactions from 50 mol % 2,2′-bis(3,4′-dicarboxyphenyl) hexafluoro propane dianhydride (6FDA) and 50 mol % 2,2′-bis(3-aminophenyl) hexafluoro propane (4,4′ 6F-diamine)(6FDAM). The details of synthesis have been reported elsewhere.[28] This polyimide polymer was very soluble in most dipolar aprotic solvents. This polymer has a glass transitional temperature of about 325°C measured by a Perkin–Elmer DSC 7 with a heating rate of 20°C/min.

Dope Preparation

6FDA/6FDAM polymeric powder (30 wt %) was dissolved in a cold DMAc solvent (0–3°C) with a high-speed stirrer. The chilled solvent reduced the dissolving rate of polyimide powder and thus prevented powders from agglomeration. The dope was then tumbled overnight at room temperature until it was fully dissolved. The spinning dope had a viscosity of 3720 poises at 30°C using a Brookfield Thermosel™ (system 3). The DMAc was chosen because it yielded a more stable solution. Figure 3 compares the stability of intrinsic viscosity (IV) curves of this polyimide as a function of time in MEK (methyl ethyl ketone) and DMAc solvents. DMAc results in a solution with a higher and more stable IV. This is due to the fact that 6FDA/6FDAM polyimide has a greater molecular interaction with DMAc than with MEK. The stability data is consistent with the calculated solubility parameter differences for these pairs. 6FDA/6FDAM has a solubility pa-

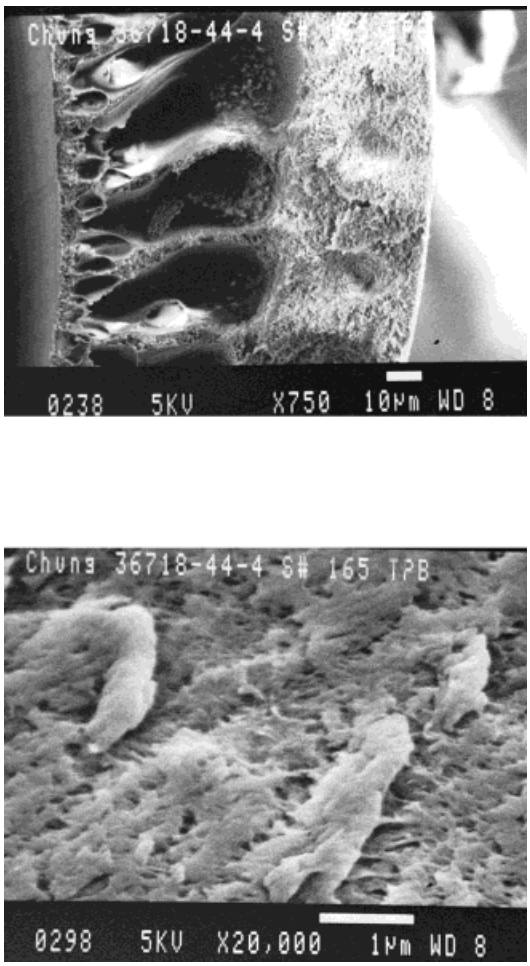

Figure 6 SEM pictures of the cross-section and external surface of fibers precipitated in 10°C (internal coagulant = 80/20 acetone/water, external coagulant = 20/80 DMAc/MeOH, 2.54 cm air-gap). Magnification: ×750 (top) and ×20,000 (bottom).

Table I Spinning Conditions for the Study of the Effects of Bath Temperature on Fiber Morphology

ID	Air-Gap Distance (cm)	Coagulation Temperature (°C)
1	2.54	3
2	2.54	10
3	2.54	20
4	2.54	32
5	2.54	42

Spinneret size A, internal coagulant = 80/20 acetone/water, external coagulant = 20/80 DMAc/MeOH; 1: A has an o.d. of 700 μm, and an i.d. of 400 μm.

rameter, δp of 11.78$(\text{cal/cc})^{0.5}$ calculated from cohesive energy tables,[29] while DMAc and MEK have δ_{solvents}, of 10.8 and 9.3 $(\text{cal/cc})^{0.5}$, respectively, obtained from a polymer handbook.[30]

Spinning Device

Figure 4 illustrates the spinning line used in this study. Dope spinning rate was controlled by a gear pump through a 6-micron filter and then to a spinneret, while the bore-fluid rate was metered by a HPLC pump (Millipore Model 501 Solvent Delivery System). A Neslab™ temperature bath was employed to control the temperature of the coagulation bath with a variation of 1°C. Two spinnerets were used; one has 700 μm outer diameter (o.d.) and 400 inner diameter (i.d.), and the other spinneret has 500 μm o.d. and 350 μm i.d. Fibers were washed in hot water (45°C) and then collected in a water tank overnight in order to remove solvent residuals.

Module Fabrication and Tests

Before fabricating a module, fibers were further immersed in methanol for solvent exchange for 0.5 h and dried. A short five-filament module was prepared to test its performance in a gas permeation cell filled with either pure oxygen or nitrogen at room temperature (25°C) during measurements. The selectivity, α, for gas A to gas B is defined as:

$$\alpha = \frac{\left(\frac{P}{L}\right)_A}{\left(\frac{P}{L}\right)_B}$$

where P/L is the permeance for gas A or gas B.[1–4] The inherent properties of this 6FDA/6FDAM polyimide have been measured from a dense film. Its oxygen permeability is 16.3 barrer and O_2/N_2 selectivity is about 4.7 at 35°C.

SEM and TEM Studies

For SEM study, the as-spun fibers were solvent exchanged in MeOH, dried, and then fractured in liquid nitrogen. For TEM examination, the samples were first embedded in epoxy and ultrathin cross sections approximately 70 nm thick were prepared using a Reichert™ ultramicrotome with a diamond knife. The thin cross-section samples were carbon coated and then examined in a JEOL 100CX TEM operating at 80 KV.

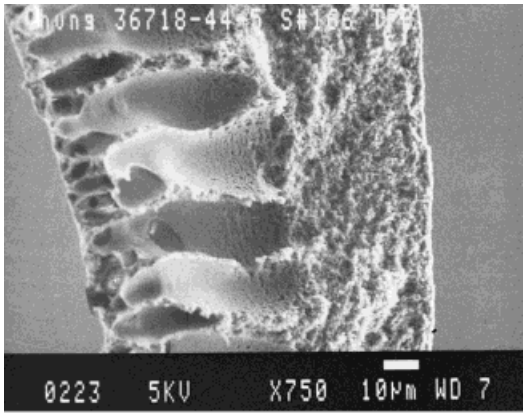

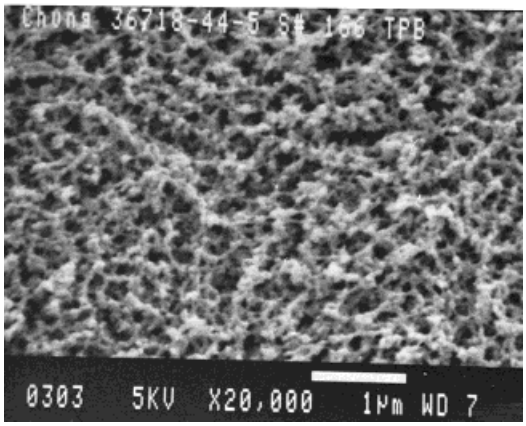

Figure 7 SEM pictures of the cross-section and external surface of fibers precipitated in 20°C (internal coagulant = 80/20 acetone/water, external coagulant = 20/80 DMAc/MeOH, 2.54 cm air-gap). Magnification: ×750 (top) and ×20,000 (bottom).

RESULTS AND DISCUSSION

The Effect of Coagulation Bath Temperature

Table I summarizes the spinning conditions for this set of experiments. Figures 5 to 9 show the effect of bath temperature on hollow-fiber cross-section structure and outer skin. All these fibers were spun with an air-gap distance of 2.54 cm. Fibers spun at low temperatures (3 and 10°C) have sharp and clear multilayer (≥3 layers) finger-like voids with a tight cross-section structure. Cross-section morphology becomes loose if the gelation bath temperature is at room temperature. A fully porous membrane is developed when the bath temperature is increased to 41°C. Compared to the fiber structure spun at 3°C, a fiber spun at 20°C has less finger-like voids. Finger-like voids disappear completely when the bath temperature are raised to 32 and 41°C. Finger-like voids are probably created by spinodal decomposition with the aid of unbalance localized stresses from surface tension, solvent/coagulant agglomeration, volumetric change, and radially convective flows of the inner and outer coagulants. When the bath temperature is increased, it results in an increase in solubilities and diffusivities. Therefore, a high bath temperature may shift the spinodal curve to the right side (polymer–coagulant axis) of the ternary phase diagram (Fig. 1) and delay the decomposition. A high bath temperature can also lower dope viscosity, chain rigidity, surface tension, and therefore reduce unbalance localized stresses that facilitate rapid decomposition during the precipitation. In addition, for a highly concentrated polymeric solution, its precipitated or

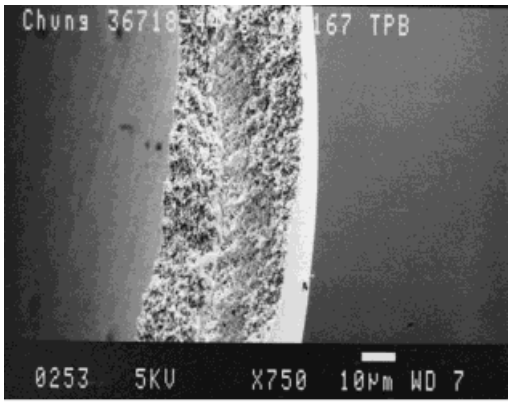

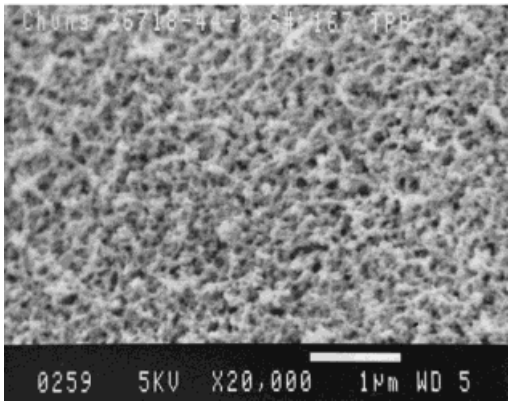

Figure 8 SEM pictures of the cross-section and external surface of fibers precipitated in 32°C (internal coagulant = 80/20 acetone/water, external coagulant = 20/80 DMAc/MeOH, 2.54 cm air-gap). Magnification: ×750 (top) and ×20,000 (bottom).

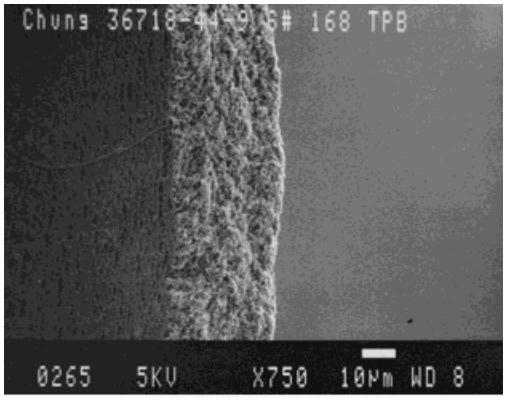

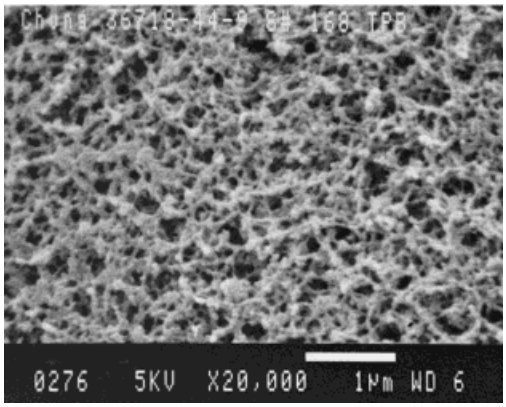

Figure 9 SEM pictures of the cross-section and external surface of fibers precipitated in 42°C (internal coagulant = 80/20 acetone/water, external coagulant = 20/80 DMAc/MeOH, 2.54 cm air-gap). Magnification: ×750 (top) and ×20,000 (bottom).

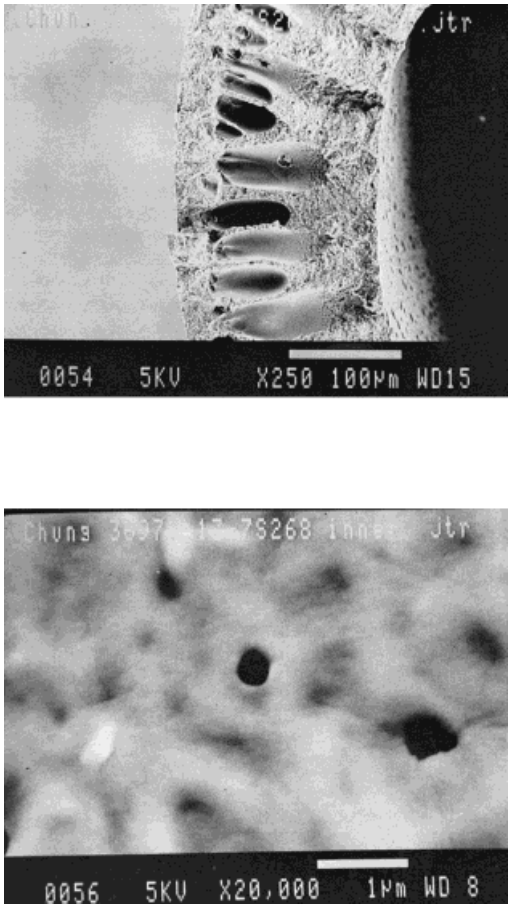

Figure 10 The effect of internal coagulant chemistry on wet-spun fiber morphology (internal coagulant = 50/50 DMAc/MeOH, external coagulant = 80/20 acetone/water, bore-fluid rate = 0.443 cc/min). Magnification: cross section (top) ×250 and inner skin (bottom) ×20,000.

gelled phase is probably more elastic at high bath temperatures (30–50°C) than at low temperatures (0–20°C). This elasticity might be able to minimize the permanent effect of deformation, caused by a rapidly spinodal decomposition, on the fiber morphology.

Figures 5 to 9 also illustrate external surface pore size distributions as a function of bath temperature. Fibers spun at 3°C have an outer skin full of 1–2 μm round pores. Pore structure changes to a three-dimensional open-cell structure if the bath temperature is equal to or greater than 20°C. This morphology change suggests that hollow fibers precipitated at 3 and 20°C have different precipitation paths. At 3°C, nascent fibers possibly went through a metastable region and then had nucleation and growth, while at 20°C, they had spinodal decomposition.

Effect of Internal Coagulants

Figures 10 and 11 show the effect of internal coagulant chemistry on fiber morphology, and Table II summarizes their process conditions. All these fibers were wet-spun into the same gelation bath at the same temperature in order to minimize the complexity induced by air gap. Because they have the same external coagulant, their external surface morphologies are quite similar; however, their finger-void (cross-section) structure, location, and internal surface morphology are remarkable difference. For a mild coagulant, such as 50/50 DMAc/MeOH mixture, the binodal and spinodal decomposition curves are possibly away from the polymer–solvent axis. When a polymeric dope precipitates in a mild coagulant, diffusion kinetics takes place first in both homogenous and metastable phases for a period of time until the dope com-

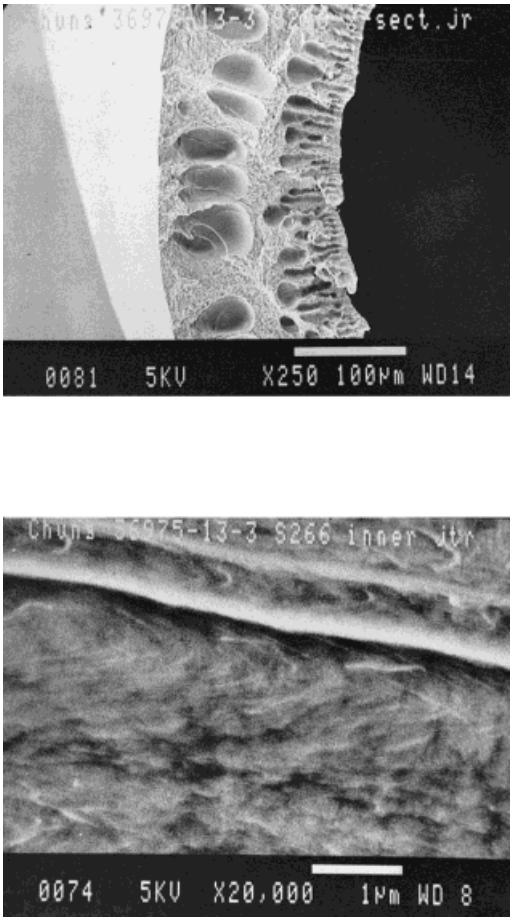

Figure 11 The effect of internal coagulant chemistry on wet-spun fiber morphology (internal coagulant = water, external coagulant = 80/20 acetone/water, bore-fluid rate = 0.437 cc/min). Magnification: cross section (top) ×250 and inner skin (bottom) ×20,000.

Table II Spinning Conditions for Study of the Effects of Internal Coagulants on Fiber Morphology

ID	Spinneret Size[a]	Dope Flow Rate (cc/min)	Flow Rate of Internal Coagulant (cc/min)	Internal Coagulant	δ Internal Coagulant $(cal/cc)^{0.5}$	External Coagulant	δ External Coagulant $(cal/cc)^{0.5}$
6	A	0.443	1.1	50/50 DMAc/MeOH	12.75[b]	80/20 acetone/H_2O	12.78[2]
7	A	0.437	1.1	H_2O	24.3[b]	80/20 acetone/H_2O	12.78[2]

No air gap, coagulation temperature, = 3–4°C.
[a] A has an o.d. of 700 μm, and an i.d. of 400 μm.
[b] Calculated at 25°C and used weight ratios during calculation for simplicity.

position reaches the spinodal decomposition curve and then thermodynamically decomposes. As a result, the finger-like voids are located a reasonable distance away from the precipitate surface (Fig. 10). For a strong coagulant, such as water, the spinodal decomposition and binodal curves are very close to the polymer/solvent axis; diffusion kinetics and thermodynamically decomposition take place almost simultaneously during the precipitation. (Strictly speaking, diffusion always occurs first and then decomposes.) The location of finger-like voids is, therefore, very close to the gelation surface of the strong coagulant, as illustrated in Figure 11. Because the polyimide dope and water have a significant difference in solubility parameter and surface tension, their compatibility is very poor. The polymer solution tends to reseal or rejoin itself even after forming finger voids. This reseal mechanism may be one of the reasons creating multiple layers of finger voids. Fiber internally coagulated by water has a pore-free inner surface, whereas fiber internally coagulated by 50/50 DMAc/MeOH has not. Only a reseal mechanism can explain the formation of multilayer finger voids with a pore-free inner surface structure.

Effect of Internal Coagulant Flow Rate

Table III summarizes the spinning conditions, and Figures 11 and 12 illustrate the effects of bore-fluid flow rate on fiber cross-section morphology and innerskin structure. Although these fibers were spun from two different spinnerets, they had almost the same dope flow rates and speed. The ratio of bore-fluid flow rates of these two fibers was about 8.46. Figure 11 clearly suggests that a higher bore-fluid rate causes a fiber with more finger voids. Table III provides the calculated bore-fluid flow speeds of these two fibers by assuming that the nascent fibers are impermeable and nondeformable. Both bore fluids move fast in their tiny bore channels within the nascent fibers. From a thermodynamic viewpoint, a system has a tendency to change its state if the change of the Gibbs free energy, ΔG, is negative, or if the change of its entropy, ΔS, is positive. Therefore, in order to lower overall system energy

Table III Spinning Conditions for the Study of the Effects of Bore-Fluid Flow Rates on Fiber Morphology

ID	Spinneret Size	Dope Flow Rate (cc/min)	Dope Flow Speed (cm/min)	Bore-Fluid Flow Rate (cc/min)	Bore-Fluid Speed[c] (cm/min)
7	A[a]	0.437	132	1.1	687.5
8	B[b]	0.170	133	0.13	106.1
Ratio				8.46	6.47

Air gap = 2.54 cm, internal coagulant = H_2O, external coagulant = 80/20 acetone/H_2O, coagulation temperature = 3–4°C.
[a] A has an o.d. of 700 μm, and an i.d. of 400 μm.
[b] B has an o.d. of 500 μm, and an i.d. of 350 μm.
[c] Inside the bore tube of the spinneret.

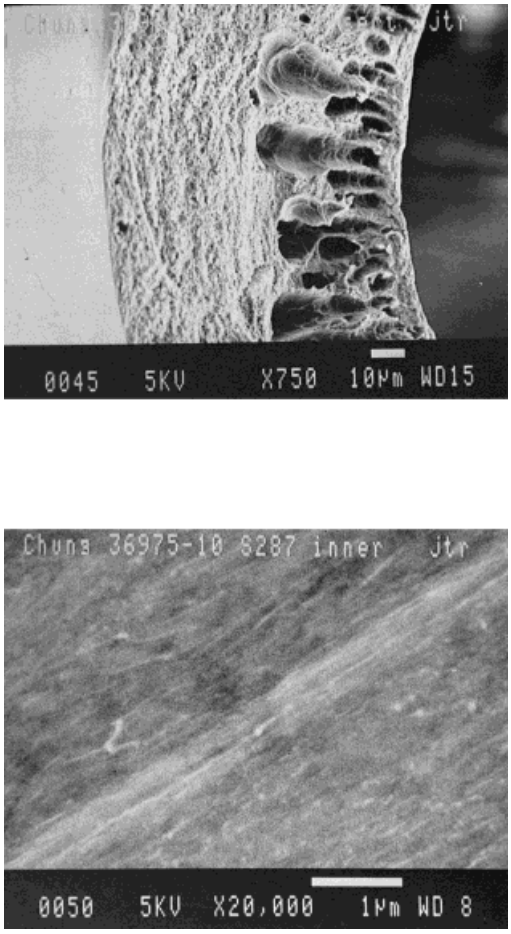

Figure 12 The effect of bore fluid rate on wet-spun fiber morphology (internal coagulant = water, external coagulant = 80/20 acetone/water, bore-fluid rate = 0.170 cc/min). Magnification: cross section (top) ×750 and inner skin (bottom) ×20,000.

or to increase system entropy, the high-speed bore fluid will introduce a radial flow through the fiber wall because the nascent fiber is flexible, permeable, and deformable.

When the bore-fluid speed is further increased, multilayer finger voids are created and fiber inner surface becomes rough, as shown in Figure 11. Because the calculated bore-fluid flow speed in the fiber of Figure 11 was of 5.47-fold higher than that of the fiber shown in Figure 12, the spinodal decomposition process might take place earlier and faster in the former than the latter. A higher bore-fluid flow speed not only created a faster solvent exchange rate, but also induced a greater and more dramatic volumetric change and unbalance localized stresses (including osmotic pressure).[31,32] More finger voids had to be produced to remove the unbalance stresses and to dissipate the overall system energy during the spinodal decomposition of a highly viscosity solution.

Effect of External Coagulants

Table IV summarizes the coagulation conditions we used to prepare this set of hollow fibers. For comparison, the internal coagulant in the first two experiments was the same and the hollow fibers were spun almost without drawing at room temperature. Figures 13 to 14 show the effects of external coagulants on the fiber cross-section morphology and external surface structure. Although both fibers are porous, they have distinct external surface structures. Fiber coagulated in 50/50 DMAc/MeOH has a few scattered pores, while fiber coagulated in 100% MeOH has an interconnected open-cell structure. This remarkable dif-

Table IV Spinning Conditions for the Study of the Effects of External Coagulants on Wet-Spun Fiber Morphology

ID	Spinneret Size[a]	Coagulation Temperature (°C)	Internal Coagulant	δ Internal Coagulant $(cal/cc)^{0.5}$	External Coagulant	δ External Coagulant $(cal/cc)^{0.5}$
9	A	4	80/20 acetone/H_2O	12.78[b]	50/50 DMAc/MeOH	12.75[b]
10	A	4	80/20 acetone/H_2O	12.78[b]	MeOH	14.7[b]
11	B	25	H_2O	24.3[b]	80/20 acetone/H_2O	12.78[b]

[a] A has an o.d. of 700 μm, and an i.d. of 400 μm; B has an o.d. of 500 μm, and an i.d. of 350 μm.
[b] Calculated at 25°C and used weight ratios during calculation for simplicity.

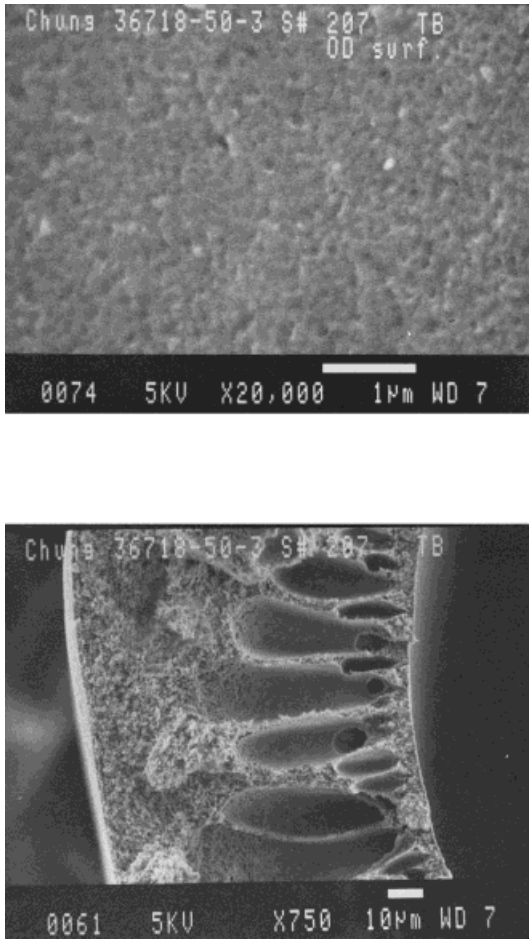

Figure 13 The effect of external coagulant, 50/50 DMAc/MeOH, on wet-spun fiber morphology (internal coagulant = 80/20 acetone/water). Magnification: outer skin (top) ×20,000 and cross section (bottom) ×750.

ference in morphology arises from the fact that their precipitation paths (kinetics and thermodynamics) are different. As illustrated in Figure 1, depending on dope composition, the flux ratio of in-flow coagulants to out-flow solvents, the locations of spinodal decomposition and binodal curves, various microporous structures can be formed during the coagulation of a hollow fiber.[9,10,14–17,22,29,33] Kinetically, MeOH is a smaller molecule than DMAc; as a consequence, the former has a much greater diffusivity and a greater flux ratio of in-flow (coagulant) to out-flow (solvent) than that of the latter. As a result, using MeOH as a coagulant tends to produce a porous membrane structure because its gelation path is closer to the solvent–coagulant axis. Thermodynamically, the solubility parameter of 6FDA/6FDAM polyimide [11.78 $(cal/cc)^{0.5}$] is closer to that 50/50 DMAc/MeOH [12.75 $(cal/cc)^{0.5}$] than that of MeOH [14.7 $(cal/cc)^{0.5}$]. This indicates that the polyimide–DMAc–MeOH ternary system should have a spinodal decomposition curve closer to the polymer–solvent axis (left-hand side) than that for the polyimide–DMAc–50/50 DMAc/MeOH system. As a result, the 6FDA/6FDAM solution precipitates faster in a MeOH solvent than in a 50/50 DMAc/MeOH mixture and has a greater opportunity in MeOH than in 50/50 DMAc/MeOH to pass the spinodal boundary to form a three-dimensional interconnected open-cell structure.

Figure 15 shows the external morphology of a 6FDA/6FDAM hollow fiber precipitated in an 80/20 acetone/water mixture. This external structure is quite similar to that of a fiber precipitated in a 50/50 DMAc/MeOH solution. Many factors

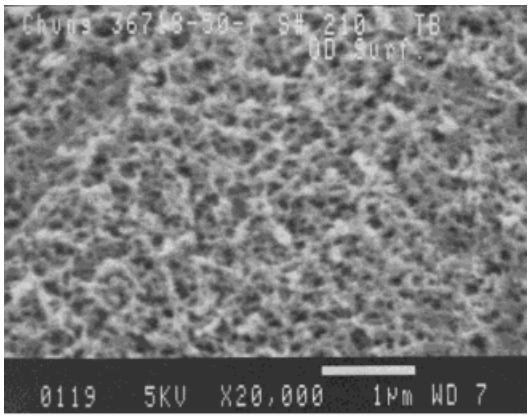

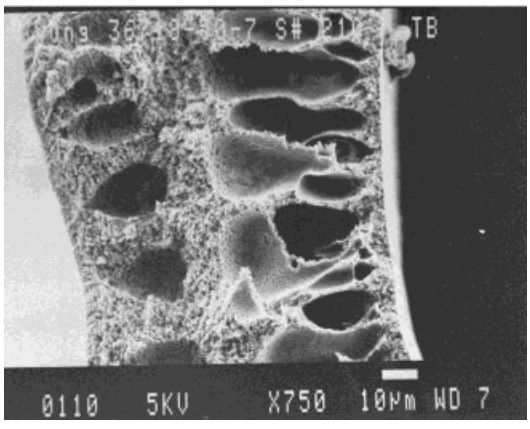

Figure 14 The effect of external coagulant, MeOH, on wet-spun fiber morphology (internal coagulant = 80/20 acetone/water). Magnification: outer skin (top) ×20,000 and cross section (bottom) ×750.

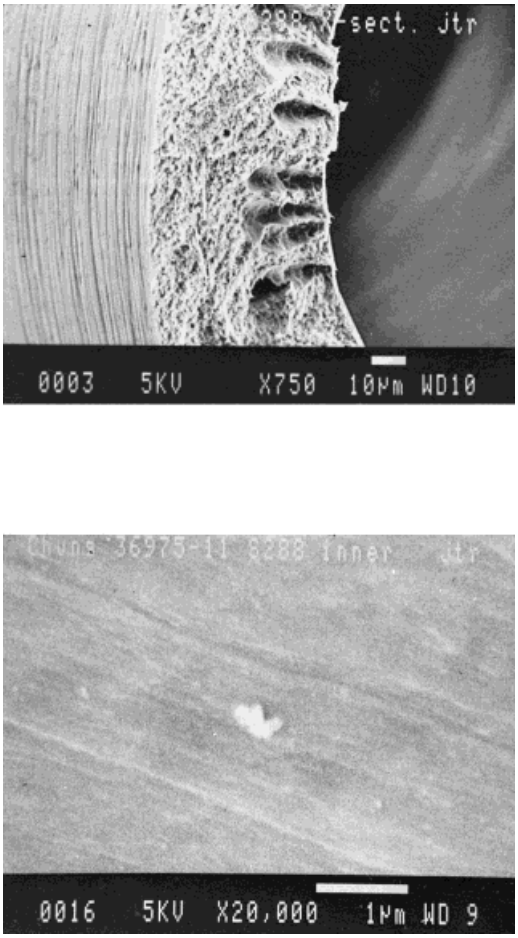

Figure 15 The effect of external coagulant, 80/20 acetone/water, on wet-spun fiber morphology (internal coagulant = water). Magnification: cross section (top) ×750 and outer skin (bottom) ×20,000, ×10,000 (right).

induce this similarity; one of them is the solubility parameter. They both have almost the same values of solubility parameter; an 80/20 acetone/water mixture has a solubility parameter of 12.78 $(cal/cc)^{0.5}$, while a 50/50 DMAc/MeOH mixture has 12.75 $(cal/cc)^{0.5}$.

Wet-spun fibers usually have a wrinkling texture on the external surface, as displayed in Figure 15. This interesting phenomenon is due to fact that die swell occurs during the extrusion of a viscous dope. The swollen extrudate shrinks and forms a wrinkling texture after leaching out the original solvent in the subsequent solvent exchange stage. As a result, wet-spun hollow fibers generally have a rougher outer surface than that of dry-jet wet-spun fibers.

The Effect of Air-Gap Distance

The effect of air-gap distance on hollow-fiber formation has been extensively studied in the previous article.[22] There is no intention to repeat it in detail here. Figures 8 and 16 show the morphology of a dry-jet wet-spun and a wet-spun fibers, respectively. The difference in morphology is mainly due to the effect of an air gap of 2.54 cm on fiber formation. The wet-spun fiber has a thicker fiber wall than the dry-jet wet-spun one. In addition, the former has an external surface morphology between a dispersed pore structure and a three-dimensional open-cell structure, while the latter has a fully three-dimensional open-cell structure. Figure 17 illustrates another example and shows that a fully three-dimensional open-cell structure

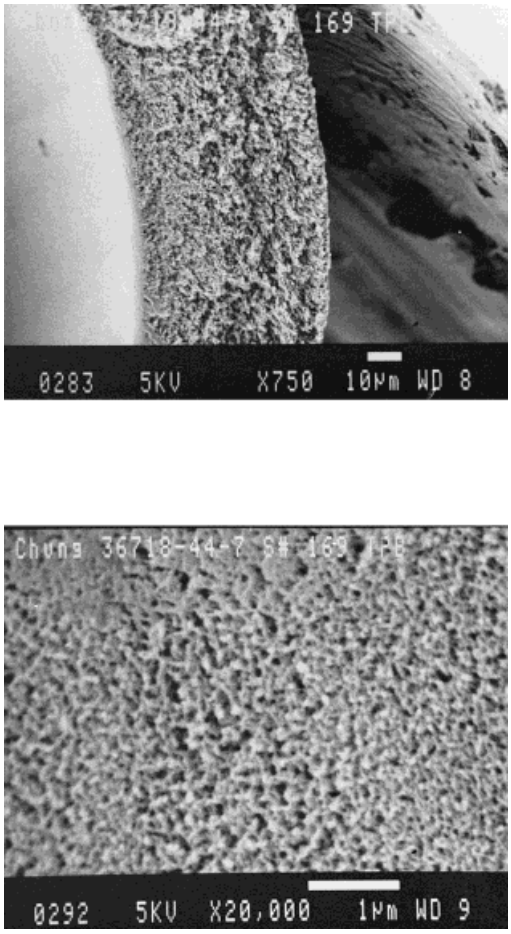

Figure 16 SEM pictures of the cross-section and external surface of wet-spun fibers precipitated in 32°C (internal coagulant = 80/20 acetone/water, external coagulant = 20/80 DMAc/MeOH. Magnification: ×750 (top) and ×20,000 (bottom).

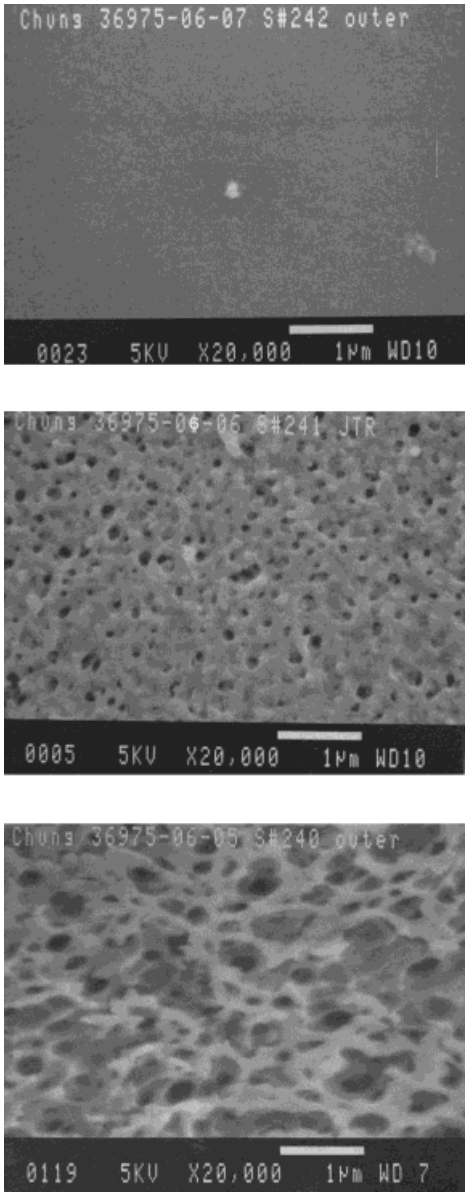

Figure 17 Effect of air-gap distance on external fiber morphology (internal coagulant = water, external coagulant = 20/80 water/acetone at 4°C). Magnification = ×20,000, top: no air-gap, middle: 2.54 cm air-gap, bottom: 12.7 cm.

can be mechanically created by an air-gap distance of 12.7 cm.[22] Therefore, air gap may have three effects on hollow-fiber formation: (1) creating extra phase instability, (2) facilitating phase separation, and (3) inducing orientation.[22] The first two effects either shorten the time for a solution moving from the binodal boundary to the spinodal boundary or reduce the distance between binodal and spinodal boundaries, while the last one results in an oriented fiber structure. As a consequence, the first two may reduce a fiber's gas/liquid selectivity because of open-cell pore formation, while the later may enhance fiber separation performance because of skin orientation (tightness). For a nascent fiber with a reasonable dope strength (elongational viscosity), one may anticipate that its gas/liquid selectivity varies with air-gap distance and there may be an optimal air-gap distance existing for the fiber separation performance.

Ripen Effect

To investigate the effect of the duration of coagulation on hollow-fiber morphology, fibers were wet-spun and immersed in coagulation baths for 30 min before taking out for sampling. Figure 18 illustrates the outer skin structures for fibers pre-

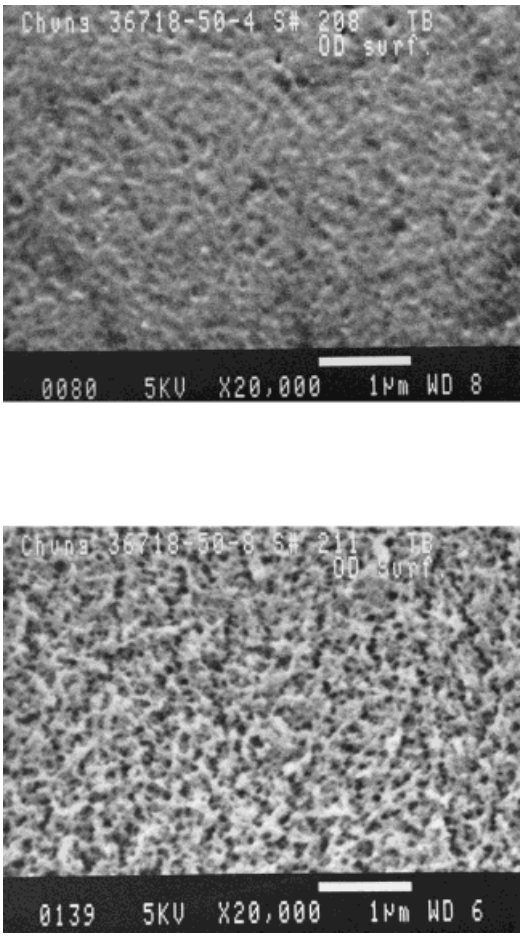

Figure 18 Fiber external morphology after immersing in coagulation baths for 30 min (internal coagulant = 80/20 acetone/water, external coagulant = top: 50/50 DMAc/MeOH, bottom: MeOH). Magnification = ×20,000.

Table V Spinning Conditions for the Study of the Effect of Air-Gap Distance on Fiber Morphology

ID	Spinneret Size[a]	Coagulation Temperature (°C)	Air-Gap Distance (cm)	Internal Coagulant	External Coagulant
12	A	32	0	80/20 acetone/H_2O	20/80 DMAc/MeOH
13	A	32	2.54	80/20 acetone/H_2O	20/80 DMAc/MeOH
14	B	4	0	H_2O	20/80 acetone/H_2O
15	B	4	2.54	H_2O	20/80 acetone/H_2O
16	B	4	12.7	H_2O	20/80 acetone/H_2O

[a] A has an o.d. of 700 μm, and an i.d. of 400 μm, B has an o.d. of 500 μm, and an i.d. of 350 μm.

cipitated in two types of nonsolvents, while Figures 13 and 14 show their corresponding fiber morphology spun at similar conditions but with a duration of about 40–80 s. The 30-min immersion does not induce a clear and visible change in external surface morphology. Although there is a slight increase in the sharpness of contour; we are not sure if it is artificial or a fact. This result implies that a wet-spun fiber develops its general structure mostly in the early stage ($<$40 s) of precipitation because of the difficulties of rearranging molecular chains in a highly concentrated and precipitated phase. This conclusion does not mean that fiber separation performance is independent of the immersion time. Previous experiments have indicated that membrane performance can be further changed by immersing it in a second coagulation bath.[34,35] This result suggests that a precipitated nascent fiber may continue its morphological change at an Angstrom-scale or nano-scale even after forming a general membrane structure.

Air-Separation Performance

Table VI summarizes the separation performance of some selective membranes. When water was used as the internal coagulant, a defect-free 6FDA/6FDAM polyimide fiber with a selectivity of 4.73 and a permeance of 38.1 GPU was produced. This fiber has a dense layer near the inner skin. Figure 19 illustrates the TEM pictures and shows that the outer skin is fully porous. Fiber separation performance decreased when 20/80 and 80/20 acetone/water mixtures were employed as the internal coagulants. This performance decrease was due to the fact that both 20/80 and 80/20 acetone/water mixtures were not so powerful as water as a coagulant. The dense

Table VI Air-Separation Performance of 6FDA/6FDAM Hollow Fibers

ID	Internal Coagulant	External Coagulant	O_2 Permeance GPU	N_2 Permeance GPU	Selectivity O_2/N_2	Dense Layer Location
11	H_2O	80/20 acetone/H_2O	38.1	8.06	4.73	inner skin
17	20/80 acetone/H_2O	80/20 acetone/H_2O	29	23	1.26	inner skin
18	80/20 acetone/H_2O	80/20 acetone/H_2O	19	14	1.35	apparently in both skins
6	50/50 DMAc/MeOH	80/20 acetone/H_2O	4.5	1.4	3.85	outer skin

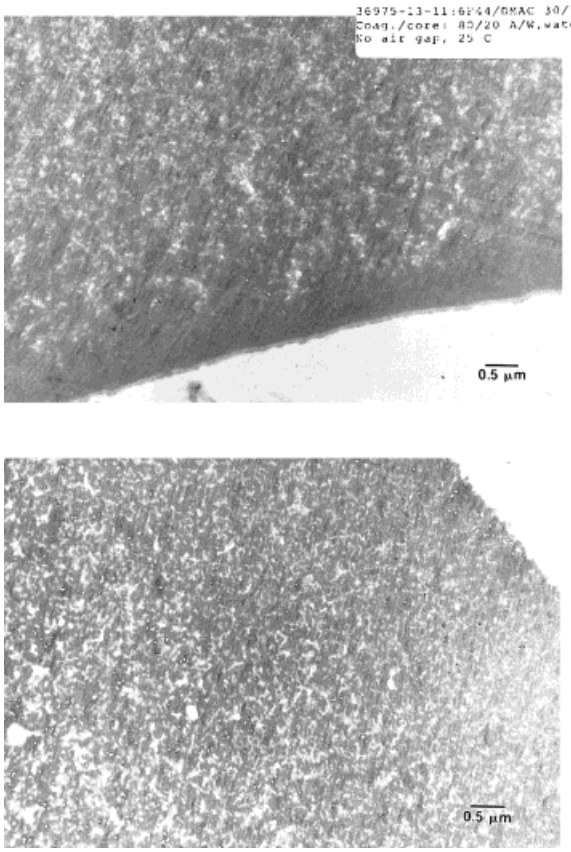

Figure 19 The TEM pictures of defect-free wet-spun 6FDA-polyimide fibers (internal coagulant = water, external coagulant = 80/20 acetone/water at 25°C). Top = cross section near the inner skin, bottom = cross section near the outer skin.

layer position shifted to the outer skin when a 50/50 DMAc/MeOH mixture was used as the internal coagulant, as illustrated in Figure 10. Because the 6FDA/6FDAM polyimide dope precipitated slowly in both 80/20 acetone/water and 50/50 DMAc/MeOH solutions, these two solvents produced fibers with thick dense layers and have extremely low permeances.

CONCLUSIONS

We have reviewed the effects of process conditions on 6FDA-polyimide hollow fibers. Experimental results indicate that solubility parameter difference, air-gap distance, and coagulation temperature have significant influence on hollow-fiber morphology and performance. An increase in air gap distance tends to induce three-dimensional open-cell pore formation. Raising coagulation bath temperature has a similar effect. Multilayer finger-void structure can be completely eliminated if one properly chooses a flow rate of internal coagulant and a gelation bath temperature. Experimental data also demonstrate that the location of the dense layer can be shifted from the inner skin to the outer skin based on the chemistry (solubility parameter) of coagulants. So does the finger-void location.

A defect-free (without silicone coating) 6FDA/6FDAM polyimide fiber with a selectivity of 4.73 and a permeance of 38.1 GPU has been developed. This fiber was wet spun from a 30/70 (weight ratio) polyimide/DMAc solution at room temperature. Water was used as the inner coagulant, while 80/20 acetone/water was employed as the outer coagulant. Fiber has an o.d. of 375 μm and i.d. of 255 μm.

The authors thank Dr. Brian W. Pengilly for his useful comments, and Drs. P. Foley, R. Chen, R. S. Kohn, R. S. Jones, and G. W. Calundann at Hoechst Celanese for providing useful help. Thanks are also due to Mr. R. H. Vora for his 6FDA/6FDAM polymer.

REFERENCES

1. T. H. Kim, W. J. Koros, G. R. Husk, and K. C. O'Brien, *J. Membr. Sci.,* **37,** 45 (1988).
2. W. J. Koros, G. K. Fleming, S. M. Jordan, T. H. Kim, and H. H. Hoehn, *Prog. Polym. Sci.,* **13,** 339 (1988).
3. S. A. Stern, Y. Mi, H. Yamamoto, and A. K. St. Clair, *J. Polym. Sci., Part B, Polym. Phys.,* **27,** 1887 (1989).
4. L. M. Robeson, *J. Membr. Sci.,* **62,** 165 (1991).
5. N. Muruganandam and D. R. Paul, *J. Membr. Sci.,* **34,** 185 (1987).
6. E. S. Sanders, Jr., J. A. Jensvold, D. O. Clark, F. L. Coan, H. N. Beck, W. E. Mickols, P. K. Kim, and W. Admassu, U.S. Pat. 4,955,993 (1990).
7. A. K. Fritzsche, M. K. Murphy, C. A. Cruse, R. F. Malon, and R. E. Kesting, *Gas Separat. Purificat.,* **3,** 106 (1989).
8. R. E. Kesting, A. K. Fritzsche, A. Cruse, M. K. Murphy, A. C. Handermann, R. F. Malon, and M. D. Moore, *J. Appl. Polym. Sci.,* **40,** 1557 (1990).
9. T. S. Chung, E. R. Kafchinski, and P. Foley, *J. Membr. Sci.,* **75,** 181 (1992).
10. T. S. Chung, R. E. Kafchinski, and R. Vora, *J. Membr. Sci.,* **88,** 21 (1994).
11. I. Pinnau and W. J. Koros, U.S. Pat. 4,902,422 (1990).
12. S. Loeb and S. Sourirajan, *Sea Water Demineralization by Means of an Osmotic Membrane,* Ad-

vances in Chemistry Series 38, American Chemical Society, Washington, DC, 1963, p. 117.
13. H. Finken, in *Material Science of Synthetic Membranes,* D. R. Lloyd, Ed., American Chemical Society, Washington, DC, 1985, p. 246.
14. K. E. Kesting, *Synthetic Polymeric Membranes,* McGraw Hill, New York, 1971.
15. H. Strathmann, K. Kock, P. Amar, and R. W. Baker, *Desalination,* **16,** 179 (1975).
16. K. Kimmerle and H. Strathmann, *Desalination,* **79,** 283 (1990).
17. W. J. Koros and I. Pinnau, in *Polymeric Gas Separation Membranes,* D. R. Paul and Y. P. Yampol'skii, Eds., CRC Press, Boca Raton, FL, 1994, p. 209.
18. D. M. Koenhen, M. H. V. Mulder, and C. A. Smolders, *J. Appl. Polym. Sci.,* **21,** 199 (1977).
19. S. Doi and K. Hamanaka, *Desalination,* **80,** 167 (1991).
20. J. Y. Lai, M. J. Liu, and K. R. Lee, *J. Membr. Sci.,* **86,** 103 (1994).
21. M. H. V. Mulder, J. O. Hendrikman, J. G. Wijmans, and C. A. Smolders, *J. Appl. Polym. Sci.,* **30,** 2805 (1985).
22. T. S. Chung, *J. Membr. Sci.,* to appear.
23. R. E. Kesting and A. K. Fritzsche, *Polymeric Gas Sparation Membranes,* John Wiley and Sons, New York, 1993.
24. D. Wang, K. Li, and W. K. Teo, *J. Membr. Sci.,* **98,** 233 (1995).
25. R. E. Kesting, A. K. Fritzsche, M. K. Murphy, A. C. Handermann, C. A. Cruse, and R. F. Malon, U.S. Pat. 4,871,494 (1989).
26. S. C. Pesek, Ph.D. Dissertation from U. of Texas, 1993.
27. S. C. Pesek and W. J. Koros, *J. Membr. Sci.,* **88,** 1 (1994).
28. T. S. Chung, R. Vora, and M. Jaffe, *J. Polym. Sci., Part A: Polym. Chem.,* **29,** 1207 (1991).
29. T. Matsuura, *Synthetic Membranes and Membrane Separation Process,* CRC Press, Boca Raton, FL, 1994.
30. J. Brandrup and E. H. Immergut, *Polymer Handbook,* VII/557, Wiley, New York, 1989.
31. S. Perez, E. Merlen, E. Robert, J. P. Cohen Addad, and A. Viallat, *J. Appl. Polym. Sci.,* **47,** 1621 (1993).
32. S. A. McKelvey and W. J. Koros, *J. Membr. Sci.,* **29,** 112 (1996).
33. L. Yilmaz and A. J. McHugh, *J. Appl. Polym. Sci.,* **31,** 997 (1986).
34. S. G. Li, G. H. Koops, M. H. V. Mulder, T. Van deb Boomgaard, and C. A. Smolders, *J. Appl. Polym. Sci.,* **94,** 329 (1994).
33. F. C. Lin, D. M. Wang, and J. Y. Lai, *J. Membr. Sci.,* **110,** 25 (1996).